

Chaotic holography in frequency downconversion

Emiliano Puddu, Alessia Allevi and Alessandra Andreoni

Dipartimento di Fisica e Matematica,

Università degli Studi dell’Insubria, via Valleggio,

11, 22100 Como, Italy and I.N.F.M.,

Unità di Como, via Valleggio, 11, 22100 Como, Italy

Maria Bondani

I.N.F.M., Unità di Como, via Valleggio, 11, 22100 Como, Italy

Abstract

We analyze and realize the recovery, by means of spatial intensity correlations, of the holographic image obtained by a difference frequency generation process in which the seed/reference field is chaotic and the object field is encoded as amplitude modulation on the pump field. Although the generated field is as chaotic as the seed field and does not carry any information about the original object, the holographic image can be extracted by measuring the spatial intensity correlations between the generated field and one Fourier component of the seed.

OCIS codes: 190.0190, 070.4340, 090.0090, 270.0270.

During the past twenty years, much theoretical and experimental work has been devoted to the study of image transfer and non-local imaging. The spatial properties of nonlinear $\chi^{(2)}$ interactions have been largely used for the realization of such experiments [1]. From a quantum point of view, the generation of couples of entangled photons by spontaneous downconversion has allowed, through coincidence techniques [2], to transfer spatial information from one of the twin photons to the other [3, 4, 5, 6]. The same techniques yielded similar results with a classical source of correlated single-photon pairs [7, 8]. It has been theoretically shown that, also in the many photon regime, image transfer can be implemented with both quantum entangled [9] and classically correlated light [10, 11, 12]. One may alternatively place the object to be imaged on the beam pumping the spontaneous parametric downconversion process [13]. Images have been actually detected by mapping suitable photon coincidences between the generated beams [14, 15, 16]. The corresponding imaging configuration in the many photon regime has not been studied yet. In this Letter, we propose a classical experiment whose aim is to mimic the many-photon quantum experiment. We realize a scheme of seeded parametric generation in which an image is encoded on the pump field, \mathbf{E}_3 (object field), and the seed field, \mathbf{E}_1 , is chaotic, being obtained from a plane wave randomized by a moving diffusing plate. We show that the generated field, \mathbf{E}_2 , is also chaotic and does not carry information about the image encoded on the pump. This interaction somehow simulates the corresponding spontaneous process, since \mathbf{E}_1 has the same chaotic statistics of the states produced by spontaneous parametric generation. Note that a plane-wave seed field \mathbf{E}_1 would generate an \mathbf{E}_2 field capable of reconstructing a holographic image of the object encoded on \mathbf{E}_3 [17, 18, 19]. Here we show that it is possible to recover such a holographic image by measuring a suitable spatial intensity correlation function between the seed/reference field \mathbf{E}_1 and the "holographic" field \mathbf{E}_2 , thus suggesting a way to extend quantum imaging protocols to the continuous-variable regime.

As shown in Fig.1 a), the amplitude modulation $U_O(x_O, y_O)$ of field \mathbf{E}_3 is obtained by placing an object-mask, O, on the beam path. The lens that is located on plane (x_L, y_L) , at distance d_F before the nonlinear crystal, images O into O' on plane (x_I, y_I) at distance $d = 2f - d_F$ beyond the crystal ($2f - 2f$ system). A plane-wave seed/reference \mathbf{E}_1 , slightly non-collinear to the pump (not shown in the figure), would generate an \mathbf{E}_2 field reconstructing a real holographic image of O' on plane (x_2, y_2) at a distance $s_2 = (k_2/k_3)d$ along the \mathbf{E}_2 propagation direction, where k_j are the wave-vector magnitudes [19]. The amplitude U_F on the plane of

the crystal entrance face (x_F, y_F) is

$$U_F(x_F, y_F) = \frac{k_3}{2\pi id} e^{i\frac{k_3}{2d}(x_F^2 + y_F^2)} \times \int dx_O dy_O U_O(x_O, y_O) e^{i\frac{k_3}{2d}\frac{d_F - f}{f}(x_O^2 + y_O^2)} e^{i\frac{k_3}{d}(x_F x_O + y_F y_O)}. \quad (1)$$

For a non depleted pump, the field complex amplitudes $a_{1,2,3}(L)$ at the crystal exit face are:

$$\begin{aligned} a_1(L) &= a_1(0) \cosh(f(\vartheta, \beta)|a_3(0)|L) \simeq a_1(0) \\ a_2(L) &= ig_{eff} L a_1^*(0) \frac{a_3(0)}{|a_3(0)|} \sinh(f(\vartheta, \beta)|a_3(0)|L) \\ &\simeq ig_{eff} L f(\vartheta, \beta) a_1^*(0) a_3(0) \\ a_3(L) &= a_3(0) = U_F(x_F, y_F), \end{aligned} \quad (2)$$

where L is the crystal thickness, $f(\vartheta, \beta)$ is a function of the propagation angles (see Fig. 1 b)), g_{eff} is the coupling constant of the interaction and the approximations hold in the low gain regime [20].

Now we consider the interaction that occurs with a chaotic $\mathbf{E}_1(\mathbf{r}) \propto \sum_{n=1}^N a_{1,n} \exp(-i \mathbf{k}_{1,n} \cdot \mathbf{r})$ having random complex amplitudes, $a_{1,n}$, and wave vectors, $\mathbf{k}_{1,n}$, with random directions but equal amplitudes, $k_{1,n} = 2\pi/\lambda_1$, for an ordinarily polarized seed/reference wave. Inside the nonlinear medium, each of the spatial Fourier components of the seed field that is phase matched with the pump generates an $a_2(L)$ contribution according to Eq. (2). Thus N holograms are simultaneously generated and the overall field is

$$\mathbf{E}_2(\mathbf{r}_{out}) \propto \sum_{n=1}^N ig_{eff} L f(\vartheta, \beta) a_{1,n}^*(0) a_3(0) e^{-i \mathbf{k}_{2,n} \cdot \mathbf{r}_{out}}, \quad (3)$$

in which $\mathbf{r}_{out} \equiv (x_{out}, y_{out}, L)$, see Fig. 1 a). Since the wave vectors $\mathbf{k}_{2,n}$ are linked to $\mathbf{k}_{1,n}$ and \mathbf{k}_3 by the phase-matching condition ($\mathbf{k}_3 = \mathbf{k}_{1,n} + \mathbf{k}_{2,n}$), they have random directions, thus impairing the hologram visibility. If we let field \mathbf{E}_2 propagate freely to the plane $(x_2, y_2, (k_2/k_3)d)$ where all N holograms do form for a type-I interaction of paraxial beams, we can calculate the intensity on that plane, which turns out to be [19, 20]

$$\begin{aligned} I_2(\mathbf{r}_2) &\propto |\mathbf{E}_2(x_2, y_2, (k_2/k_3)d)|^2 \\ &= \left| \sum_{n=1}^N c_n a_{1,n} U_O(x_{2,n} - x_2, y_{2,n} - y_2) \right|^2 \\ &= \sum_{n=1}^N |c_n|^2 |a_{1,n}|^2 |U_O(x_{2,n} - x_2, y_{2,n} - y_2)|^2, \end{aligned} \quad (4)$$

where the coefficients $|c_n|^2$ summarize all constant factors and the transverse translations, $x_{2,n}$ and $y_{2,n}$ (if refraction at the exit face of the crystal is neglected: $x_{2,n} = (k_2/k_3)d \sin \beta_{2,n}$ and $y_{2,n} = (k_2/k_3)d \cos \beta_{2,n} \sin \vartheta_{2,n}$, see Fig. 1 b)) are due to the different directions of the $\mathbf{k}_{2,n}$ wave vectors. In the last expression in Eq. (4) the intensity $I_2(\mathbf{r}_2)$ could be written as the sum of N terms because, owing to the incoherence of the N components of \mathbf{E}_2 , all the interference terms vanish. The observation that each term of the sum is proportional to the intensity of the n -th reference field component, $|a_{1,n}|^2$, provides a means to recover the holographic image. In fact, if we calculate the spatial correlation function of the intensity $I_{1,j} = |a_{1,j}|^2$ of a single component of the seed with the intensity map of the generated field, $I_2(x_2, y_2, z_2)$, we get:

$$\begin{aligned}
G(I_{1,j}, I_2) &= \langle I_{1,j} I_2 \rangle - \langle I_{1,j} \rangle \langle I_2 \rangle \\
&= \langle |a_{1,j}|^2 \sum_{n=1}^N |c_n|^2 |a_{1,n}|^2 |U_O(x_{2,n} - x_2, y_{2,n} - y_2)|^2 \rangle \\
&\quad - \langle |a_{1,j}|^2 \rangle \langle \sum_{n=1}^N |c_n|^2 |a_{1,n}|^2 |U_O(x_{2,n} - x_2, y_{2,n} - y_2)|^2 \rangle \\
&= \sum_{n=1}^N |c_n|^2 |U_O(x_{2,n} - x_2, y_{2,n} - y_2)|^2 \\
&\quad \times (\langle |a_{1,j}|^2 |a_{1,n}|^2 \rangle - \langle |a_{1,j}|^2 \rangle \langle |a_{1,n}|^2 \rangle) \\
&= \sum_{n=1}^N |c_n|^2 |U_O(x_{2,n} - x_2, y_{2,n} - y_2)|^2 \sigma^2(|a_{1,n}|^2) \delta_{j,n} \\
&= |c_j|^2 \sigma^2(I_{1,j}) |U_O(x_{2,j} - x_2, y_{2,j} - y_2)|^2, \tag{5}
\end{aligned}$$

where $\langle \dots \rangle$ is the ensemble average. In deriving Eq. (5) we neglected the pump fluctuations and used the property of chaotic light: $\langle |a_{1,j}|^2 |a_{1,n}|^2 \rangle - \langle |a_{1,j}|^2 \rangle \langle |a_{1,n}|^2 \rangle = \sigma^2(|a_{1,n}|^2) \delta_{j,n}$, in which $\sigma^2(|a_{1,j}|^2) \equiv \sigma^2(I_{1,j})$ is the variance. This result shows that $G(I_{1,j}, I_2(x_2, y_2))$ is proportional to the intensity map of the difference-frequency generated holographic image of the object $|U_O|^2$ "recorded" by the j -th component of the seed/reference field \mathbf{E}_1 . For an experimental proof, we have to map $I_2(\mathbf{r}_2)$ and to measure $I_{1,j}$, which is easily done by using a lens and mapping $I_1(\mathbf{r}_1)$ in its focal plane.

The experimental setup is sketched in Fig. 2. The wavelengths of the interacting fields are $\lambda_1 = \lambda_2 = 1064$ nm, $\lambda_3 = 532$ nm. Pump and seed fields are obtained from a Nd:YAG laser (10 Hz repetition rate, 7-ns pulse duration, Quanta-Ray GCR-4, Spectra-Physics Inc., Mountain View, CA). The nonlinear crystal is a type I β -BaB₂O₄ crystal (cut angle 32 deg,

cross section 10 mm \times 10 mm and 4 mm thickness, Fujian Castech Crystals Inc., Fuzhou, China). The detection planes of $I_{1,j}$ and $I_2(\mathbf{r}_2)$ are made to coincide on the sensor of the same CCD camera (Dalsa CA-D1-256T, 16 $\mu\text{m} \times 16 \mu\text{m}$ pixel area, 12 bits resolution, operated in progressive scan mode), so that each signal occupies half sensor. The chaotic reference field \mathbf{E}_1 is generated by passing the beam at λ_1 through a ground-glass diffusing plate, which is moved shot by shot, by selecting a portion of diffused light with an iris, PH, of ~ 8 mm diameter and finally by filtering the ordinary polarization with a polarizing beam splitter, PBS, and a half-wave plate. Lens L_2 ($f = 15$ cm) provides the Fourier transform of \mathbf{E}_1 . To check the chaotic nature of this seed/reference field we measured the probability distribution, $P_r(I_1)$, of the intensity recorded by the different CCD pixels for a single shot, and the probability distribution, $P_t(I_1)$, of the intensity recorded by a single pixel for many successive laser shots (see Fig. 2, inset). The good agreement with thermal distributions show that \mathbf{E}_1 is actually randomized in space at each shot and that any $I_{1,j}$ is random from shot to shot. The desired imaging configuration was realized by using a copper mask with three holes ($\sim 256 \mu\text{m}$ diameter) as the object O , and by recording $I_2(\mathbf{r}_2)$ at the laser repetition rate. The intensity correlation function in Eq. (5) was evaluated over 1000 shots by taking the whole map $I_2(x_2, y_2)$ and by selecting the value of a single pixel in the intensity map of I_1 . In Fig. 3 a), we show the resulting reconstructed image (map of $G(I_{1,j}, I_2(x_2, y_2))$), to be compared with the conventional real-time hologram obtained in single shot upon removing the light diffusing plate, Fig. 3 b). The similarity in the quality of the two images is really impressive, in particular if the reconstructed image is compared with a single-shot intensity map $I_2(x_2, y_2)$, Fig. 3 c), and with the average intensity map $\langle I_2(x_2, y_2) \rangle$ of the 1000 repetitions, Fig. 3 d).

In conclusion, we have demonstrated that the spatial intensity correlation properties of the downconversion process can be used to recover a selected image from a chaotic ensemble of holographic images. The image recovered by $G(I_{1,j}, I_2(x_2, y_2))$ fulfils the holographic properties of the difference-frequency generated hologram that would be obtained by using the single plane-wave $\mathbf{E}_{1,j}$ as the seed/reference field [17, 18, 19]. We expect that the method also works in the case of an unseeded process in the continuous-variable regime, in which the selection of a single spatial and temporal frequency in the parametric fluorescence cone should determine the position of the reconstructed holographic image.

[1] M. I. Kolobov, Rev. Mod. Phys. **71**, 1539-1589 (1999).

[2] B. E. A. Saleh, A. F. Abbouraddy, A. V. Sergienko, and M. C. Teich, Phys. Rev. A **62**, 043816 (2000).

[3] A. V. Belinskii and D. N. Klyshko, JETP **105**, 259-262 (1994).

[4] P. H. S. Ribeiro, S. Padua, J. C. Machado da Silva and G. A. Barbosa, Phys. Rev. A **49**, 4176-4179 (1994).

[5] D. V. Strekalov, A. V. Sergienko, D. N. Klyshko, and Y. H. Shih, Phys. Rev. Lett. **74**, 3600-3603 (1995).

[6] G. A. Barbosa, Phys. Rev. A **54**, 4473-4477 (1994).

[7] R. S. Bennink, S. J. Bentley, and R. W. Boyd, Phys. Rev. Lett. **89**, 113601 (2002).

[8] R. S. Bennink, S. J. Bentley, and R. W. Boyd, Phys. Rev. Lett. **92**, 033601 (2004).

[9] A. Gatti, E. Brambilla, and L. A. Lugiato, Phys. Rev. Lett. **90**, 133603 (2003).

[10] J. Cheng, and S. Han, Phys. Rev. Lett. **92**, 093903 (2004).

[11] A. Gatti, E. Brambilla, M. Bache, and L. A. Lugiato, Phys. Rev. A. **70**, 013802 (2004).

[12] D. Magatti, F. Ferri, A. Gatti, M. Bache, E. Brambilla, and L. A. Lugiato, arXiv:quant-ph/0408021.

[13] A. F. Abouraddy, B. E. E. Saleh, A. V. Sergienko, and M. C. Teich, J. Opt. Soc. Am. B **19**, 1174-1184, (2002).

[14] T. B. Pittman, Y. H. Shih, D. V. Strekalov, and A. V. Sergienko, Phys. Rev. A **52**, R3429-R3429 (1995).

[15] C. H. Monken, P. H. S. Ribeiro, and S. Padua, Phys. Rev. A **57**, 3123-3126 (1998).

[16] D. P. Caetano, P. H. S. Ribeiro, J. T. C. Pardal, and A. Z. Khoury, Phys. Rev. A **68**, 023805 (2003).

[17] A. Andreoni, M. Bondani, Yu. N. Denisyuk, and M. A. C. Potenza, J. Opt. Soc. Am. B **17**, 966-972 (2000).

[18] M. Bondani and A. Andreoni, Phys. Rev. A **66**, 033805 (2002).

[19] M. Bondani, A. Allevi, A. Brega, E. Puddu and A. Andreoni, J. Opt. Soc. Am. B **21**, 280-288 (2004).

[20] M. Bondani, A. Allevi, E. Puddu and A. Andreoni, manuscript in preparation.

List of Figure Captions

Fig. 1. a) Propagation scheme. b) Interaction inside the crystal, optical axis on the shaded plane.

Fig. 2. Experimental setup: HS, harmonic separator; D, diffusing plate; M_{1-5} , mirrors. Lens L_1 , which images O into O' , forms a $2f - 2f$ system. Lens L_2 provides the spatial Fourier transform of \mathbf{E}_1 . All distances are in cm. Inset: logarithmic plot of the probability distributions $P_{\mathbf{r},t}(I_1)$.

Fig. 3. a) Map of $G(I_{1,j}, I_2(x_2, y_2))$ evaluated on 1000 shots. b) Conventional holographic image. Chaotic holographic images: c) single-shot and d) average over 1000 shots.

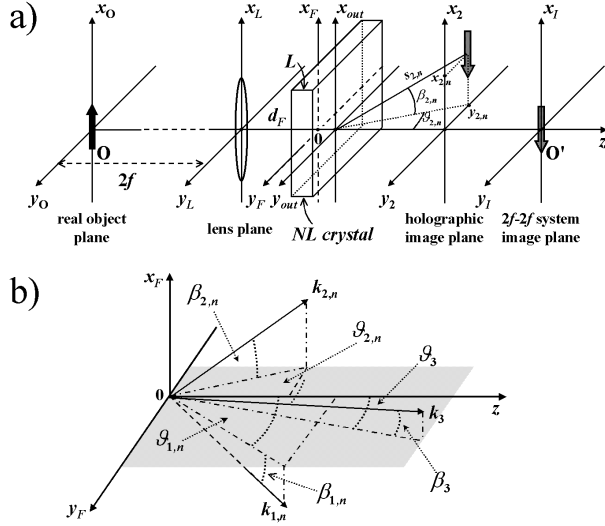


FIG. 1: a) Propagation scheme. b) Interaction inside the crystal, optical axis on the shaded plane.
fig1.eps.

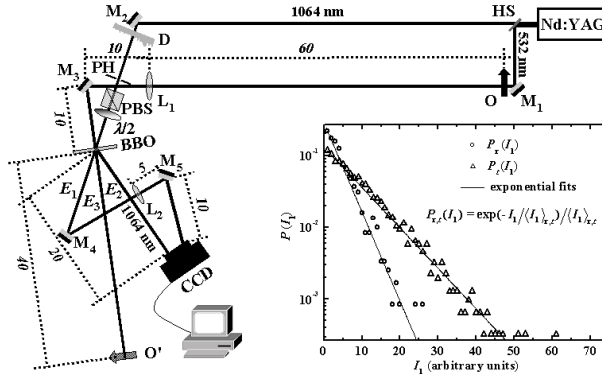


FIG. 2: Experimental setup: HS, harmonic separator; D, diffusing plate; M₁–₅, mirrors. Lens L₁, which images O into O', forms a 2f – 2f system. Lens L₂ provides the spatial Fourier transform of \mathbf{E}_1 . All distances are in cm. Inset: logarithmic plot of the probability distributions $P_{r,t}(I_1)$.
fig2.eps.

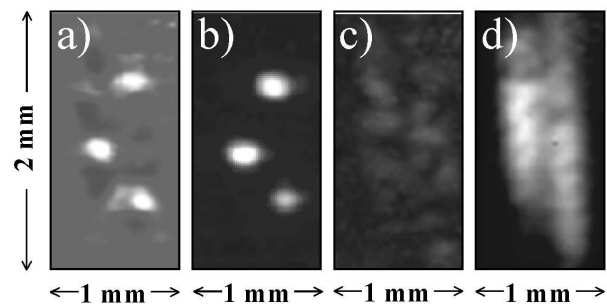


FIG. 3: a) Map of $G(I_{1,j}, I_2(x_2, y_2))$ evaluated on 1000 shots. b) Conventional holographic image. Chaotic holographic images: c) single-shot and d) average over 1000 shots. fig3.eps.